EVALUATION OF NUMERICAL APPROACHES FOR THE DEVELOPMENT OF INTERLAMINAR DAMAGE IN COMPOSITE LAMINATES

Alessandro Airoldi*, Giuseppe Sala*, Paolo Bettini*
***Department of Aerospace Engineering, Politecnico di Milano, Italy**

Keywords: *Interface Elements, Interlaminar Toughness, Interlaminar Strength, Composites, Failure analysis*

Abstract

The paper presents the application of a numerical approach to evaluate both the onset as well the propagation of interlaminar damages in composite laminates using finite element explicit analyses. An interface constitutive model is applied within a modeling technique developed to include the interlaminar layers in the finite element schemes of composite laminates. The possibility to model a laminate with different levels of mesh refinement through the laminate thickness is assessed The capability to model the nucleation of interlaminar damage in quasi-static tests is then evaluated considering short beams tests performed on specimens made of fabric composites. The approach is then applied to model the interlaminar damages and failures obtained in bending experiments performed on thick composite specimens. The development of interlaminar fractures in undamaged specimens, their propagation modes and the failure loads appear to be correctly modeled by the approach.

1 Introduction

A critical aspect in the design and the analysis of composite structures is the need to identify the potential locations of interlaminar damage nucleation and to evaluate the risk of interlaminar crack propagation under prescribed load conditions.

Conventional finite element stress analyses can identify critical interlaminar stress states in a laminate presenting variations of geometry, cut-outs or free-edge effects, but such strength based approaches are not adequate to analyze the risk of crack propagation in the structure. An alternative to the adoption of fracture mechanics methodologies is represented by the application of interface elements that exploit the peculiar characteristics of the interlaminar fracture process. The composite laminate may, in fact, modeled at the meso-scale level as an assembly of plies connected by interfaces and properly formulated constitutive law can model the delamination process in such interfaces, assuming that the process zone is small and translates without modifications [1, 2]. Interface elements have been developed and assessed by many authors with appreciable results either considering quasi-static loading conditions [3,4,5,6,7] as well as the development of delamination in impact conditions [8,9].

According to the results presented in literature, the technique seems suitable to forecast the onset and to analyze the mode of propagation of interlaminar damage in composite structures, even without an a-priori identification of the most critical zones for the development of interlaminar cracks. To accomplish such objective, the paper adopts an approach based on finite element explicit analyses, to easily handle with strain softening behavior of the material, high velocity crack propagation and contact phenomena. A technique is moreover developed to model the interlaminar phase in composites parts at different mesh refinement levels through the thickness of the laminate. The basic aspects and a preliminary assessment of the technique are presented. The application of the method to the analysis of the failures obtained in short beam tests is subsequently described, discussing the role of the material parameters in the numerical computation. Finally, the approach is applied to thick specimens made of carbon fabric layers in bending conditions, considering cases where the variation of the lay-up sequences and the applied transverse loads have induced the development of interlaminar damage.

2 Modelling technique

2.1 Basic Aspects

The approaches based on interface elements consider the composite laminate as an assembly of laminae connected by interfaces, where interlaminar damage nucleates and develops. The fracture process is described by using, as kinematic variables, the displacement discontinuities at an arbitrary material point belonging to an interface surface (Fig 1-A). Within this scheme, a zero-thickness interface element, endowed with a properly formulated traction-displacement law, can be used to model the interlaminar damage.

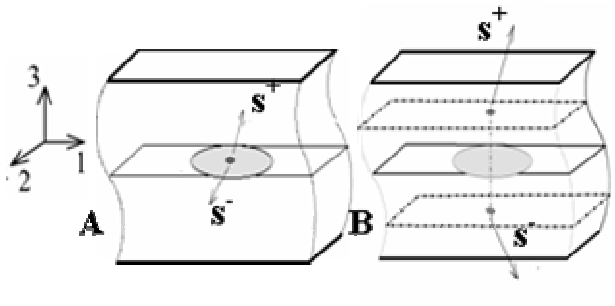

Fig. 1. Description of interlaminar fracture in the interface (A) and in the proposed (B) approach

In the proposed approach, a composite laminate is considered as an assembly of sublaminates, to be modeled by means of bi-dimensional elements. The kinematic variables used to describe the fracture process in mode I, II and III are the relative displacements at the mid-planes of the sublaminates (Fig. 1-B), described by the vector $\{\Delta\}$ given in Eq. 1.

$$\begin{Bmatrix} \Delta_I \\ \Delta_{II} \\ \Delta_{III} \end{Bmatrix} = \begin{Bmatrix} S_3^+ - S_3^- \\ S_1^+ - S_1^- \\ S_2^+ - S_2^- \end{Bmatrix} \tag{1}$$

Within a small strain assumption, the vector $\{\Delta\}$ can be related to the average value of the out-of-plane components acting in the material volume between the sublaminates with thickness *th* (Eq. 2).

$$\begin{aligned} \{\varepsilon\} &= \{\varepsilon_{33} \quad \gamma_{13} \quad \gamma_{23}\}^T \\ \{\varepsilon\} &= \{\Delta\}/th \end{aligned} \tag{2}$$

Such a description, in a finite element scheme, leads to model the out-of-plane elastic and inelastic response of the composite by means of a solid element having a null in-plane response (Fig. 2). The adoption of a linear 8-nodes element with a reduced integration scheme assures that the response is indeed described in terms of the average strain state between the sublaminates connected by the solid.

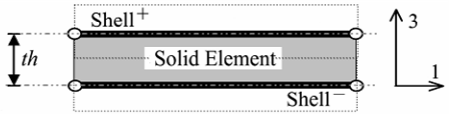

Fig. 2. Modelling technique for a composite laminate

A constitutive law with damage can be attributed to the solid to model the interlaminar fracture process, as shown in Eq. 3.

$$\begin{Bmatrix} \sigma_{33} \\ \sigma_{13} \\ \sigma_{23} \end{Bmatrix} = \begin{bmatrix} E_{33} & 0 & 0 \\ 0 & G_{13} & 0 \\ 0 & 0 & G_{33} \end{bmatrix} (1-d) \begin{Bmatrix} \varepsilon_{33} \\ \gamma_{13} \\ \gamma_{23} \end{Bmatrix} \tag{3}$$

The onset and the evolution of the damage variable can be set to model the strength and the toughness of the interlaminar layers. To accomplish such objective, the approaches based on the interface elements typically exploit the links between the critical energy release rates and the energy dissipated in the damage process [1]. The same procedure can be followed in the proposed approach, taking into consideration the relationship between the displacement vector $\{\Delta\}$ and the average strain $\{\varepsilon\}$, given in Eq. 2, so that Eqs. 4 are obtained.

$$\begin{aligned} \int_0^\infty \sigma_{33} d\Delta_I &= th \int_0^\infty \sigma_{33} d\varepsilon_{33} = G_{I\,c} \\ \int_0^\infty \sigma_{13} d\Delta_{II} &= th \int_0^\infty \sigma_{13} d\gamma_{13} = G_{II\,c} \\ \int_0^\infty \sigma_{23} d\Delta_{II} &= th \int_0^\infty \sigma_{23} d\gamma_{23} = G_{II\,Ic} \end{aligned} \tag{4}$$

A simplifying hypothesis is introduced throughout this work, considering that all the properties relevant to fractures developing in mode II and mode III are identical. This allows to define two stress components acting in the interlaminar layer and driving the fracture process determined by tensile (mode I) and shear stress (mode II) (Eq. 5).

The strength of the interlaminar layer is modeled using a quadratic criterion [10] calibrated

on the basis of the strength σ_I^0 and σ_{II}^0, referred to a fracture process evolving in pure mode *I* and *II*, respectively (Eq. 6).

$$\sigma_I = \begin{cases} 0 & if\ \sigma_{33} \le 0 \\ \sigma_{33} & if\ \sigma_{33} > 0 \end{cases} \qquad \sigma_{II} = \sqrt{\sigma_{13}^2 + \sigma_{23}^2} \tag{5}$$

$$\sqrt{\left(\frac{\sigma_I}{\sigma_I^0}\right)^2 + \left(\frac{\sigma_{II}}{\sigma_{II}^0}\right)^2} = 1 \tag{6}$$

The damage evolution law are determined imposing a bi-linear response to the stress-strain curve of the material, as shown in Fig. 3, and using Eq. 4 to identify the final strain ε_I^F and ε_{II}^F that define the energy absorbed in the damage process.

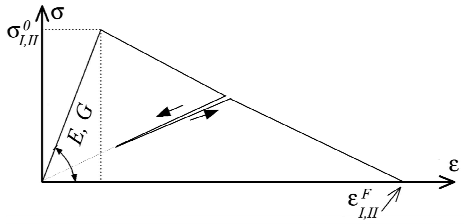

Fig. 3. Stress-strain response of the interlaminar material model

Different formulations have been proposed to take into account the toughness in mixed mode fracture process. The formulation proposed for the interface elements in [6] has been chosen in this work and has been introduced in the material model attributed to the elements that represent the interlaminar phase. According to the chosen model, the toughness in mixed mode is determined by a quadratic toughness criterion, expressed as in Eq. 7.

$$\sqrt{\left(\frac{G_I}{G_{Ic}}\right)^2 + \left(\frac{G_{II}}{G_{IIc}}\right)^2} = 1 \tag{7}$$

It is worth noting that, in the constitutive response, damage does never influence the compressive stiffness, E_{33}, so to model the contact between adjacent plies even when the interlaminar layer is completely damaged. The obtained material model for the interlaminar layers has been implemented in a FORTRAN subroutine to be linked to the HKS/Explicit Code [11].

2.2 Preliminary assessments of the modeling approach

The proposed technique can be adopted to model a laminate by dividing it into sublaminates connected by interlaminar layers. The finite element schemes can thus be developed at different mesh refinement levels through the laminate thickness, as all the interlaminar layers between the plies can be considered or only few layers can be modeled between a set of selected sublaminates. In order to assess the capability of such an approach to correctly represent the basic aspects of a composite laminate behavior, the finite element model of a 50 mm long, 10 mm wide and 2.95 mm thick carbon fabric plate has been developed and solved with HKS/Abaqus Explicit. The plate model has been considered clamped at one end and loaded at the opposite end by a transverse shear load. An homogeneous $[0/90]_{12}$ lay-up sequence of fabric plies, with E_{11}=E_{22}=62.5 GPa and a cured ply thickness of 0.246 mm, has been considered. The values of G_{13} and G_{23} have been set to 4.0 GPa.

The mesh has been developed with a 2.5 mm x 2.5 mm grid on the laminate plane. A shell model of the laminate, without interlaminar layers, has been used as reference. The technique has then been assessed by comparing the results of the reference model with the ones of models including an increasing number of interlaminar layers, *N*, and adopting different types of bi-dimensional elements (shells *S4R* and membrane *M3D4R* [11]). The interlaminar layers have been modeled with *C3D8R* elements [11]. Table 1 summarizes the characteristics of the models.

Table 1. Developed models of a clamped laminate for the assessment of the technique

#	N	2D element	$\frac{Dof}{Dof_0}$	Solid aspect ratio	CPU time / CPU time$_0$
0	0	Shell	1.0	-	1.0
1	1	Shell	2.0	1.7	1.2
2	5	Shell	6.0	5.1	7.4
3	5	Membrane	3.0	5.1	3.5
4	11	Membrane	6.0	10.2	12.1

Two types of analyses have been carried out with two different time histories of the applied load: a triangular impulse with a duration of 1 ms and an amplitude of 50 N (case A) and a terminated ramp, raising from 0 to 50 N in 5 ms (case B).

The numerical time histories of the free end displacement are given in Fig. 4. It can be observed that the differences between the bending responses of the models are absolutely negligible. Hence, the obtained results indicate that the application of the technique does not modify the bending stiffness of a laminate and also that solid elements with a very high aspect ratio can be adopted to model the interlaminar layers. The ratio of the required computational time to the one of the reference model is also given in Table 1 for the case A.

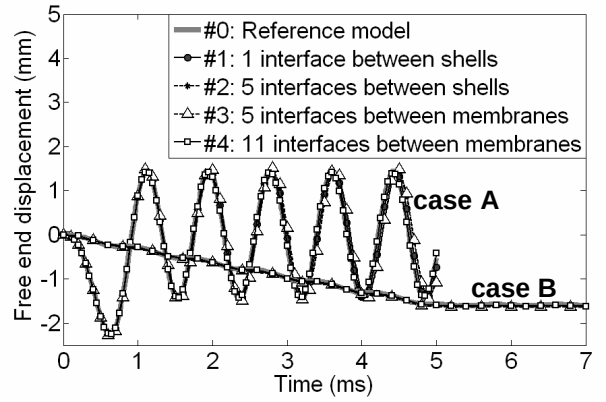

Fig. 4. Numerical bending responses of models with different mesh refinement levels

3 Nucleation and propagation of interlaminar damage in short beam tests on fabric specimens

The approaches based on interface elements have been proved particularly effective to model the propagation of interlaminar damages. The prediction of the onset and of the subsequent propagation of the interlaminar damage is actually complicated by the need to accurately model the interlaminar stress state through the laminate thickness. The short beam test can be considered one of the simplest, though inaccurate, method to evaluate the interlaminar properties of composites laminates. The reasons for the test inaccuracy can be found considering the conditions of load application that lead to stress distributions different from the nominal solution expected by applying a beam theory [12]. For the same reason, this simple test represent a particularly interesting benchmark to evaluate the possibility to model the nucleation and propagation of delamination in undamaged composite laminates.

3.1 Test Results

Short beam tests have been carried out on specimens manufactured with a vacuum-bag process using a plane weave fabric pre-preg, with T800 carbon fibers and an Hexcel 1947 epoxy resin. The specimens, having a length of 40 mm and a width of 12 mm have been cut from a 6.16 mm thick laminate with a $([0][90])_{7S}$ lay-up. Figure 5 shows the loading nose and the supports used in the test, with a diameter of 5.8 mm and of 3.0 mm, respectively.

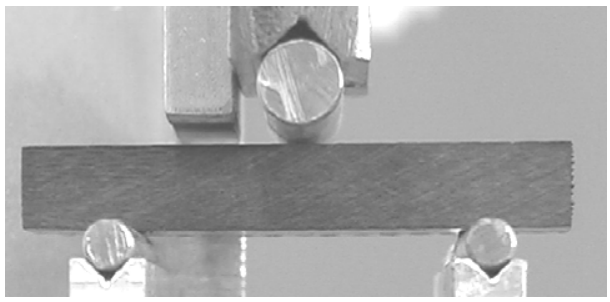

Fig. 5. Set-up of the short beam test

The test have been performed with a MTS Alliance RF/200 static test system adopting a cross-head speed of 1 mm/min. The load vs. displacement curves obtained in three tests are presented in Fig. 6. An average maximum load of 6.4 kN has been reached during the test, followed by a sudden load drop. All the specimens retained a not negligible load carrying capability after the failure, at a load level between 4 kN and 2 kN.

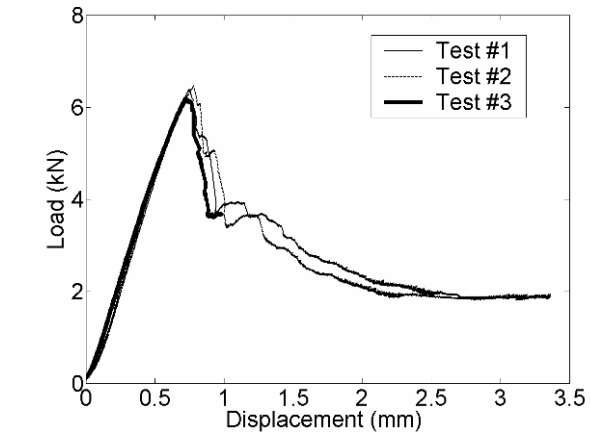

Fig. 6. Experimental force vs. displacement curves in the short beam tests

As shown in Fig. 7, failures have occurred between one of the support and the loading nose. Although no visible damage can be detected in Fig. 7-B, referred to an instant immediately after the failure, a series of interlaminar cracks are clearly seen in Fig. 7-C, showing the specimen at the end of the test. The picture presented in Fig. 8-A shows the detail of the failed zone

In order to evaluate the interlaminar damage immediately developed after the failure, the third test has been arrested just after the load drop. The specimen has then been analysed by means of dye

penetrant inspection. The result, reported in Fig. 8-B, indicates that the pattern of interlaminar cracks, characterising the failure of these specimen, is indeed fully developed immediately after the failure.

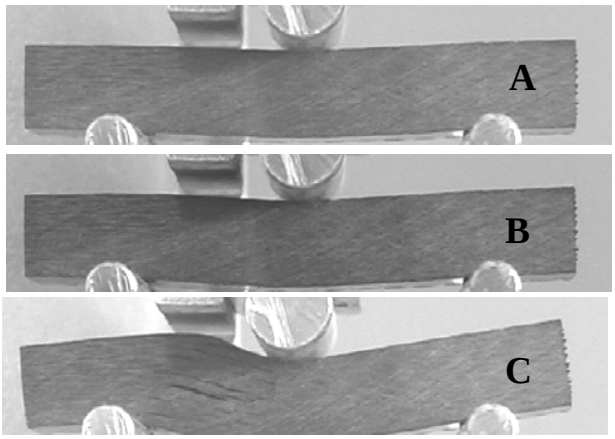

Fig. 7. Short beam specimen immediately before the failure (A), immediately after the failure (B) and at the end of the test (C)

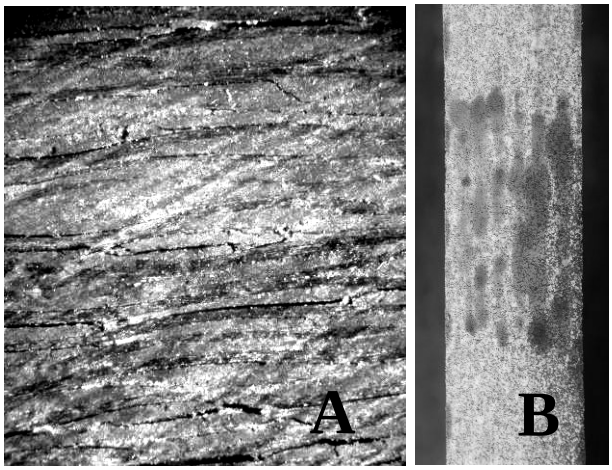

Fig. 8. Detail of the failed zone at the end of the test (A) and dye penetrant inspection of a specimen immediately after the failure (B)

3.2 Numerical analyses

The model of the short beam test has been developed with the proposed numerical approach adopting a mesh refinement at the ply level. All the 28 plies of the laminate have been represented by shell elements, connected by 27 layers of solid elements. Symmetry has been exploited modeling only half of the specimen with a total number of 21560 elements (Fig. 9). Rigid surfaces have been used to represent the loading nose and the supports, interacting by means of penalty contact algorithms with the specimen surface. The explicit finite element analyses have been performed imposing a velocity boundary condition to the loading nose and choosing the velocity level so to avoid dynamic oscillations during the loading phase.

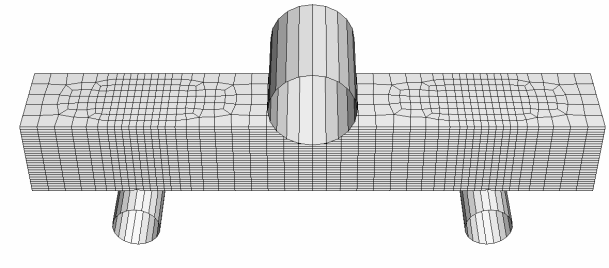

Fig. 9. Numerical model of the short beam test

Table 2 reports the in-plane tensile and compressive stiffness of the material, evaluated by characterisation tests. The out-of-plane shear stiffness $G_{13}=G_{23}$ has been set to 2.0 GPa by correlating the numerical and experimental slopes of the force vs. displacement curve in the loading phase. The interlaminar shear strength, σ_{II}^{0}, has been preliminarily evaluated by applying the approximate formulation proposed in [13] and set to 65.0 MPa.

The ultimate load and the damage distribution obtained in the numerical analyses have been found influenced by the value of the interlaminar tensile strength, σ_{I}^{0}, that has been consequently identified by means of a sensitivity study and eventually set to 17.2 MPa.

Table 2. In-plane stiffness of the composite plies

	E_{11} (GPa)	E_{22} (GPa)	G_{12} (GPa)	ν_{12} (-)
Tensile	76.0	76.0	4.03	0.07
Compressive	68.4	68.4		

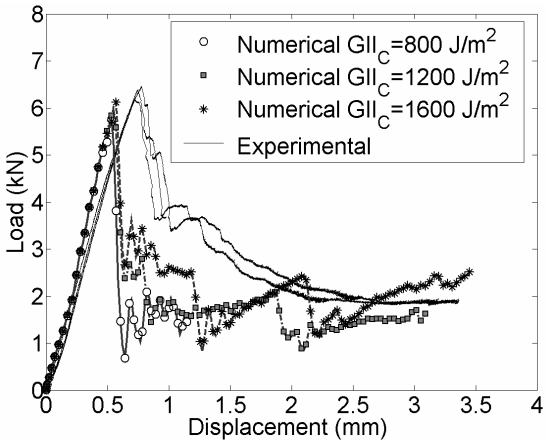

Fig. 10. Numerical-experimental correlation obtained varying G_{IIc} and using σ_{II}^{0}=65.0 MPa, σ_{I}^{0}=17.2 Mpa, G_{Ic} = 120 Jm^{-2}

Figure 10 reports the numerical-experimental correlation obtained using the selected strength values and setting the critical energy release rate in mode I, G_{Ic}, to 120 Jm^{-2}, while G_{IIc} has been varied in the range 800 Jm^{-2} ÷ 1600 Jm^{-2}. The correlation shown in Fig. 10 until the specimen failure is acceptable. Discrepancies can be observed in the loading phase, probably due to the difficulty to model the contact and the friction between the laminate and the cylinders as well as to possible non-linearities in the transverse shear response of the material. The maximum load is as well slightly underestimated, but the load drop is correctly predicted and a residual load carrying capability after the failure is obtained. Such residual load level increases with the toughness attributed to the material model. Figure 11 reports the contour of the interlaminar damage obtained in the analyses with G_{IIc}=1200 Jm^{-2} at different deflection levels. The analysis of the damage evolution can be summarized in the following points:

i - damage develops quite early in the analysis below the load application cylinders, but does not propagate;

ii - a localized damage appears before the failure at a corner of the loading nose;

iii – damage spreads at failure along an inclined band and a pattern of fully developed interlaminar cracks appears, in agreement with the experimental evidence;

iv - in the subsequent evolution some of these cracks propagates until the edge of the specimen.

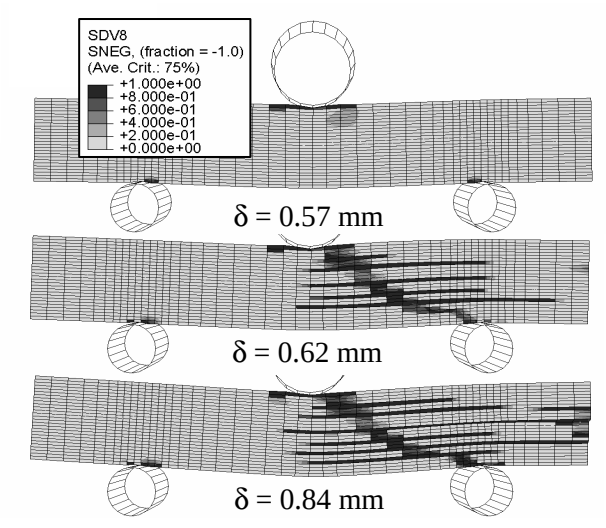

Fig. 11. Evolution of interlaminar damage using σ_{II}^0=65.0 MPa, σ_I^0=17.2 Mpa, G_{Ic} = 120 Jm^{-2} and G_{IIc} = 1200 Jm^{-2}

The comparison between the damage evolution obtained using G_{IIc}=800 Jm^{-2} and G_{IIc}=1600 Jm^{-2} allows to evaluate the role played by the interlaminar toughness (Fig. 12). The analysis with the lower toughness tends to anticipate the development of failures. Moreover, a lower number of fully developed interlaminar crack is obtained and the cracks develop immediately until the edge of the specimen. Comparing the numerical results with the experimental evidence, it can be observed that a G_{IIc} higher than 1200 Jm^{-2} is required to obtain a failure mode in agreement with the experimental results. It should also be observed that the damage evolution obtained in the final phase of the analysis with G_{IIc} = 1200 Jm^{-2} may be significantly influenced by the undamped high frequency oscillations of the model after the energy release subsequent to the failure.

The aforementioned influence of the σ_I^0 value on the maximum load level reached in the numerical computation can be explained observing the stress contour reported in Fig. 13, referred to the analysis with G_{IIc}=1200 Jm^{-2}. The interlaminar shear stress distribution is characterized by a stress concentration near the loading nose (Fig. 13-A) but, when the interlaminar damage starts developing, as shown in Fig. 11 at δ=0.57 mm, a zone characterized by tensile values of σ_{33} up to 15 MPa appears in front of the nucleating crack (Fig. 13-B).

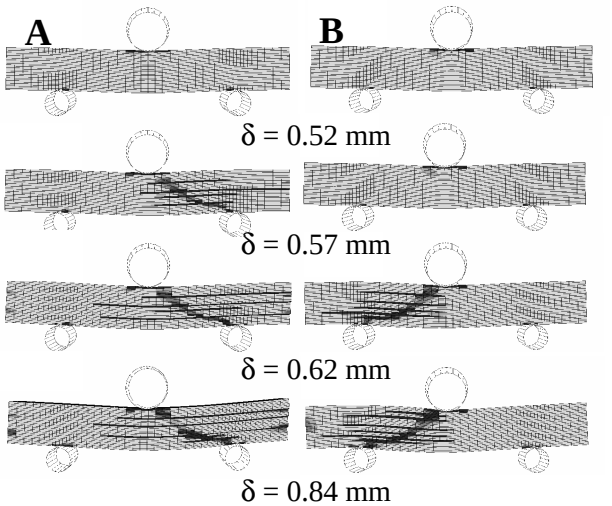

Fig. 12. Evolution of interlaminar damage using σ_{II}^0=65.0 MPa, σ_I^0=17.2 Mpa, G_{Ic} = 120 Jm^{-2} G_{IIc} = 800 Jm^{-2} (A) and G_{IIc} =1600 Jm^{-2} (B)

The results reported in Fig. 14, obtained raising σ_I^0 to 25.0 MPa and setting the ratio between G_{Ic} and G_{IIc} to 0.2, confirm that the numerical maximum load and the residual load are indeed increased by varying the properties relevant to the interlaminar

properties in mode I. However, Fig. 15 indicates that these modifications significantly change the damage development in the numerical model as few interlaminar cracks, rapidly developing until the edge of the specimen, are obtained, whichever level of G_{IIc} is adopted.

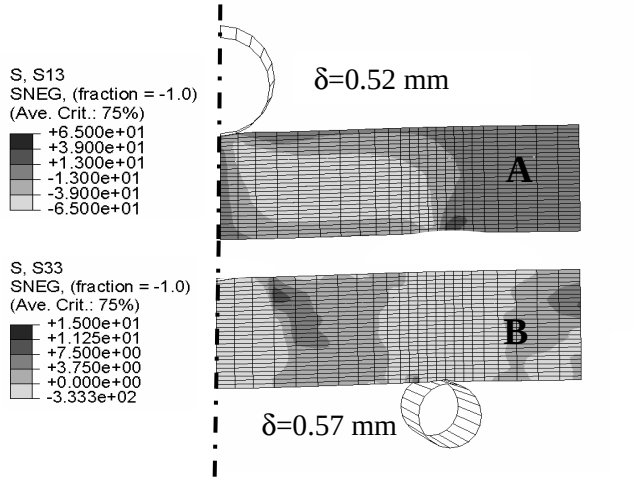

Fig. 13. Contour of interlaminar shear stress (A) and of tensile interlaminar stress (B) at failure

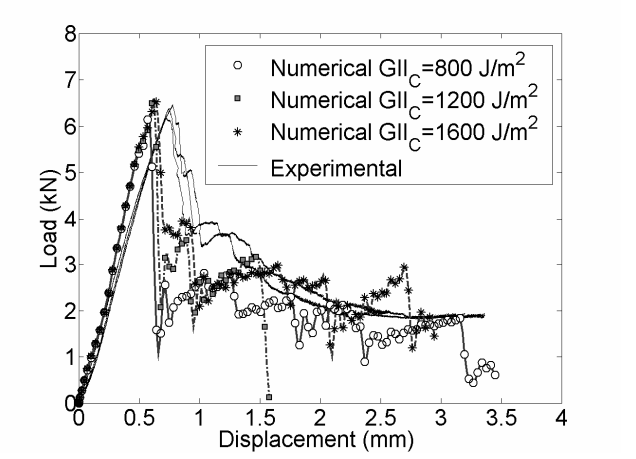

Fig. 14. Numerical-experimental correlation obtained varying G_{IIc} and using σ_{II}^0=65.0 MPa, σ_I^0=25.0 Mpa, G_{Ic}/ G_{IIc} = 0.2

4 Application of the approach to bending experiments on thick tapered specimens

4.1 Experimental results

The previously presented results indicate that the proposed approach can be successfully applied to model the nucleation and the propagation of interlaminar damage in undamaged specimens in presence of complex stress states. Accordingly, the technique has been adopted to analyze two bending experiments, performed on elements manufactured with the same material system of the specimen tested with the short beam method. Two types specimens have been considered, both having a width of 36 mm and presenting a tapered zone with a transition from a lay-up having fibers in the 0°, 90° and +/-45° direction to a pure cross-ply lay-up, as shown in Fig. 16-A. Averagely, the specimen thickness in the transition zone varies from 11.30 mm to 6.23 mm. The first specimen has been tested in a three points bending condition (Fig. 16-B), while a four points bending test has been performed on the second one, as indicated in Fig. 16-C.

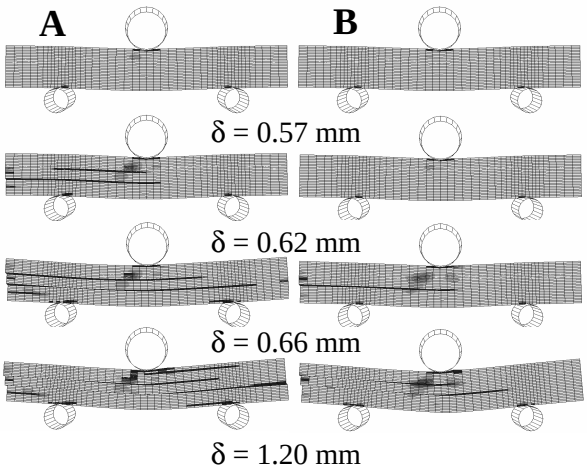

Fig. 15. Evolution of interlaminar damage using σ_{II}^0=65.0 MPa, σ_I^0=25.0 Mpa, G_{Ic}/G_{IIc} = 0.2, and G_{IIc} =800 Jm^{-2} (A) and G_{IIc} =1600 Jm^{-2} (B)

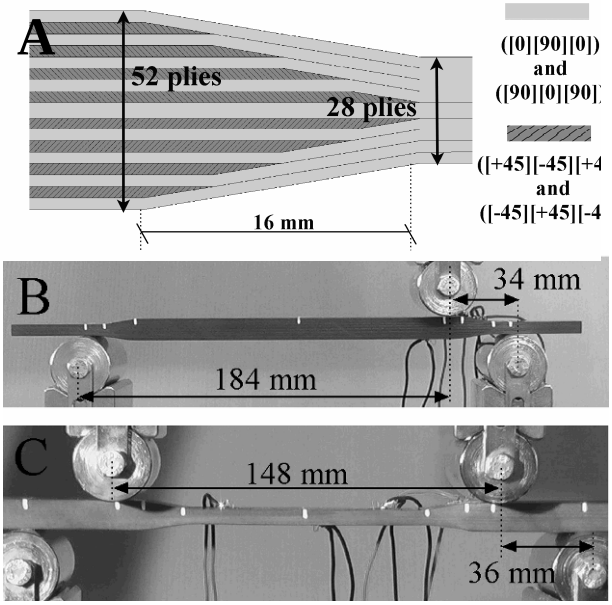

Fig. 16. Detail of the transition zone in the tapered specimens (A) and set-up of the three points (B) and of the four points bending test (C).

The tests have been performed with an MTS Alliance RF/200 static test system at a cross head speed of 1.0 mm/mm. Loads have been applied by means of steel cylinders with a diameter of 30 mm. Figure 17 reports the average curves obtained in the three valid tests carried out in the two experimental configurations and shows that data scattering can be considering acceptable, with the exception of a single test in the three point bending configuration.

The response of the specimens have been in both cases influenced by the development of interlaminar damages. In the three point bending test, failure has been actually caused by the development of interlaminar cracks nucleated between the loading central cylinder and the support. An instantaneous loss of load carrying capability has been observed in correspondence of the development of a major interlaminar crack at the mid-plane of the specimen, although minor interlaminar damages have developed in the transition zone during the prosecution of the test (Fig. 18). As far as the four points bending test is concerned, the nucleation and the stable propagation of an interlaminar crack in the lower part of the transition zone has been observed in all the three performed tests (Fig. 19-A). The average load corresponding to the detection of this interlaminar damage has been reported in Fig. 17. The maximum load carried by the specimen has always been slightly higher and has been determined by the compressive failure of the fabric plies (Fig. 19-B).

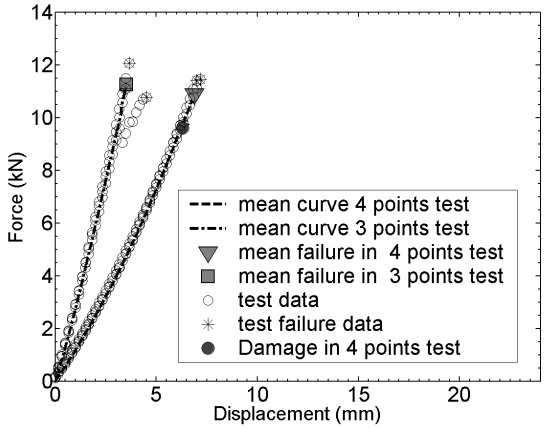

Fig. 17 – Average force vs. displacement curves obtained in the bending experiments

Fig. 18 – Failure in the three point bending test

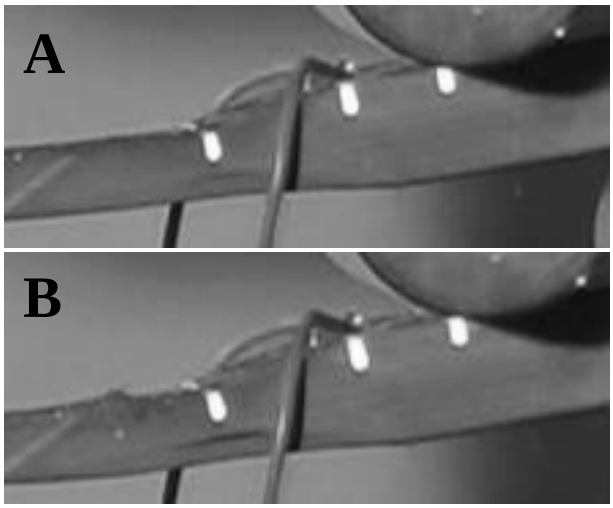

Fig. 19 – Interlaminar damage nucleation (A) and failure (B) in the four points bending test

4.2 Numerical analyses

The models of the bending experiments have been developed choosing a mesh refinement at the sublaminate level, using a single layer of shells to represent each group of 0°/90° an +/-45° fabric plies in the lay-up sequence (Fig. 16-A). Accordingly, 9 and 17 sublaminates have been modelled in the thin and in the thick parts of the specimens, respectively. Figure 20 shows the detail of the modeled transition zone. The results of preliminary analyses, performed without activating the damage in the constitutive law, have been used to evaluate the stress states in the models. In the three points bending analyses, the maximum interlaminar shear stress is obtained at the mid-plane of the specimen, in the thin part, as shown in Fig. 21-A. The stress history presented in Fig. 21-B, at the point indicated by the star symbol in Fig. 21-A, shows that a pure mode II delamination is forecasted by the model. In the four points bending test, at the location indicated by the star symbol in Fig. 22-A, a tensile interlaminar stress is observed, in correspondence of the damage nucleated in the tests. The stress history at this point (Fig. 22-B) indicates that the interlaminar shear reaches as well critical values, so that a mixed mode delamination can be expected according to the numerical results.

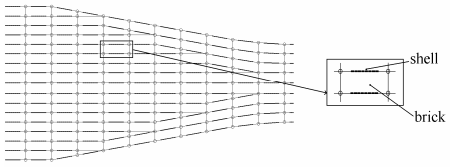

Fig. 20. Detail of the transition zone in the numerical models of the specimens

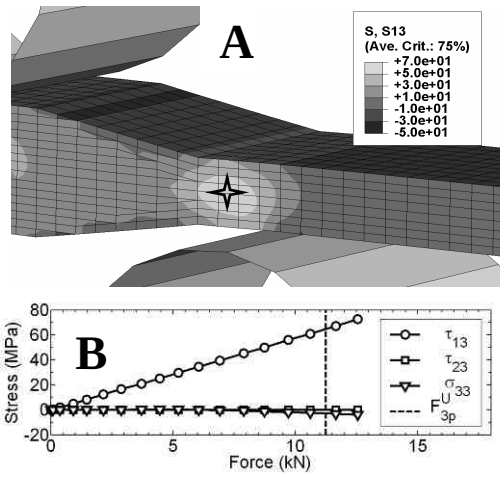

Fig. 21. Contour of stress component σ_{13} in the analysis of the three-points bending test (A) and stress vs. force curves in an element (B)

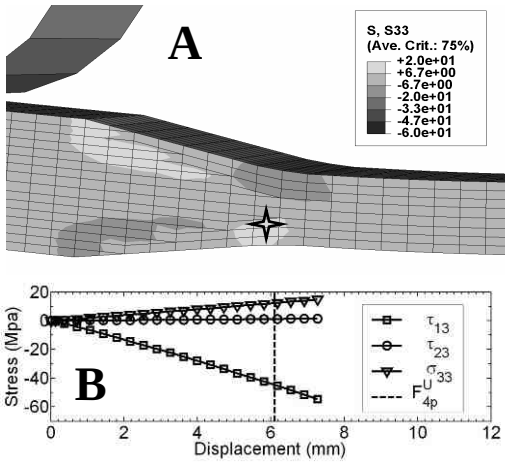

Fig. 22. Contour of stress component σ_{13} in the analysis of the four-points bending test (A) and stress vs. displacement curves in an element (B)

From the quantitative point of view, the observed stress levels have confirmed the strength values attributed to the interlaminar elements in the previously presented analyses of the short beam tests. Hence, the σ_I^0 and σ_{II}^0 values have been set to 17.2 MPa and 65.0 MPa, respectively. As far as the toughness is concerned, the best numerical-experimental correlation has been globally obtained using G_{Ic} = 120 Jm^{-2} and G_{IIc} =1200 Jm^{-2}. Figure 23 reports the numerical-experimental correlation obtained in all the analyses performed with the selected set of material parameters , including the result referred to the short beam test.

The evolution of the interlaminar damage in the analyses of the three points bending test is reported in Fig. 24. Damage nucleates below the central cylinder and, before the failure, propagates towards the transition zone. Such a type of damage has been also obtained in the tests as shown in Fig. 18. Failure is obtained in correspondence of δ = 3.38 mm. The subsequent evolution leads to a numerical damage that appears in good agreement with the experimental evidence, although it is worth noting that the experimental final state, shown in Fig. 18, has been obtained prosecuting the test after the initial load drop, meanwhile a sudden propagation has been obtained in the numerical computation as it can be evaluated by analyzing Fig. 24 and the numerical force vs. displacement curve.

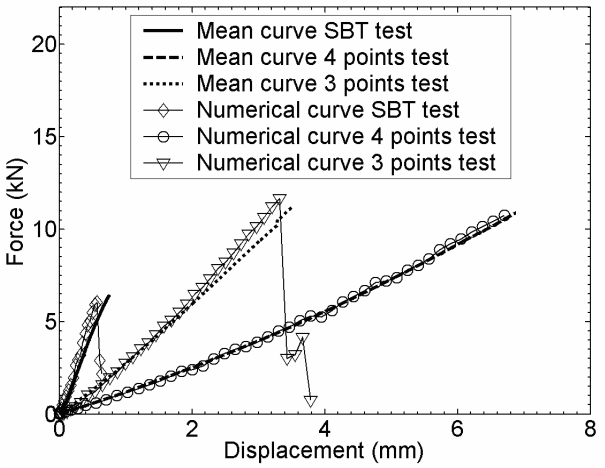

Fig. 23. Overall numerical-experimental correlation obtained with the selected set of material parameters

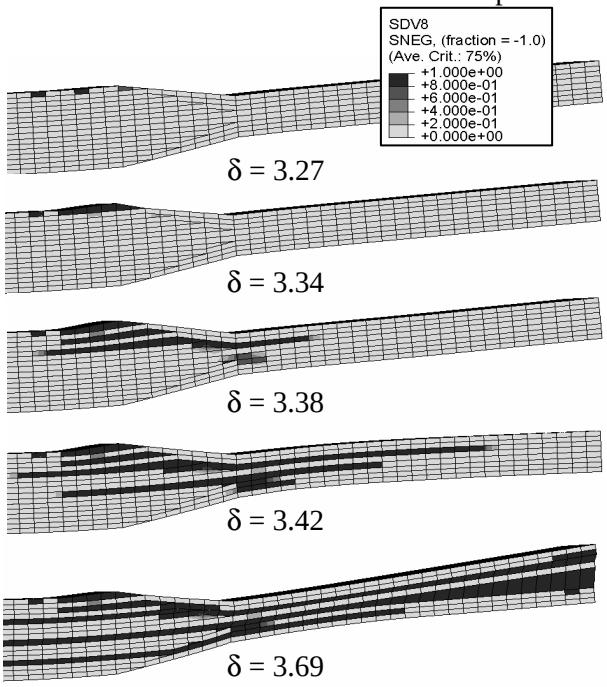

Fig. 24. Evolution of interlaminar damage in the three points bending test

In the four points bending tests, failure has not been caused by interlaminar damages, but the numerical analysis has correctly modeled the nucleation and the stable propagation of the interlaminar crack in the transition zone, as shown in Fig. 25.

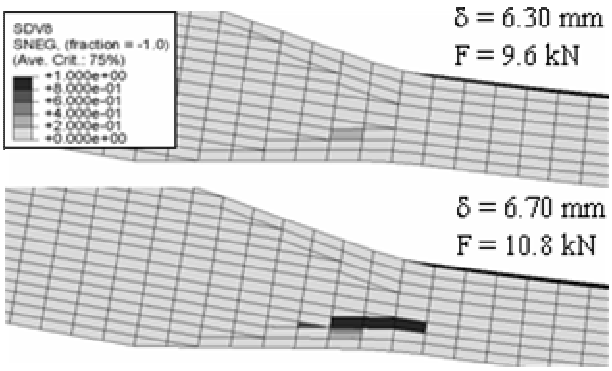

Fig. 25. Stable evolution of the interlaminar damage in the four points bending test

5 Conclusions

The nucleation and the propagation of interlaminar damages in composite laminates have been modeled by means of a numerical approach based on an interface constitutive law. The law has been applied within a modeling technique suitable to model the interlaminar layers at the required mesh refinement level through the laminate thickness. Finite element explicit analyses have been performed adopting the approach and considering three different types of tests. The interlaminar strength levels of the material have been evaluated by analyzing the numerical stress distributions and the effect of the interlaminar toughness have been investigated by means of sensitivity analyses. The identified set of material parameters has obtained for all the tests a good agreement as far as the overall force vs. displacement response of the specimen is concerned. Moreover, the onset of delamination, the stable propagation of interlaminar damages and the complex damage distribution obtained at the failure of the specimens, are in good agreement with the experimental evidences, although the numerical models generally tend to overestimate the length of the cracks propagating in unstable mode. The effect of friction, of strain rate sensitivity and of the undamped high frequency oscillations can be investigated to explain such behavior. Other improvements and the evaluation of the mesh sensitivity of the results could be considered to develop a reliable method for the design and the analysis of composite structures taking into account the risk of interlaminar damage nucleation and propagation.

References

[1] Allix O., Leveque D., Perret L., “Identification and forecast of delamination in composite laminates by an interlaminar interface model”, *Composite Science and Technology*, Vol. 58, pp. 671-678, 1998.

[2] Corigliano A., “Formulation, identification and use of interface models in the numerical analysis of delamination”. *Int. J. Solids and Structures*, VOl. 30, pp. 2779-2811, 1993.

[3] Mi Y., Criesfiled M. A., Davies G. A., Hellweg H. B.,”Progressive delamination using interface elements”, *Journal of composite materials*, Vol. 32, No. 14, pp. 1246-1272, 1998.

[4] Reedy E. D. Jr, Mello .F. J., Guess T. R., ”Modeling the initiation and growth of delamination in composite structures, *Journal of Composite Materials*, Vol. 31, No. 8, pp.812-831, 1997.

[5] De Moura M., Goncalves J., Marqus A., de Castro P., “Modelling compression failure after low velocity impact on laminated composite materials using interface elements”, *Journal of Composite Materials*, Vol. 31, pp. 1462-1479, 1997.

[6] Davila C., “Mixed mode decohesion elements for analyses of progressive delaminations”, *42nd AIAA/ASME/ASCII/AHS/ASC Structures, Structural Dynamics, and Material Conference and Exhibit*, Seattle, WA, USA, 16-19 April 2001.

[7] Bianchi S., Corigliano A., Frassine R., Rink M., Modelling of interlaminar fracture process in composite using interface elements, *Composite Science and Technology*, Vol. 66, pp. 255-263, 2006.

[8] Wisheart M., Richardson M. “The finite element analysis of impact induced delamination in composite materials using a novel interface element”, *Composite Part A*, Vol. 29A, pp. 301-303, 1998.

[9] Johnson A., Holzpapfel M., “Modeling of soft body impact on a composite structure”, *Composite Strucutres*, Vol. 61, pp. 103-113, 2003.

[10] Brewer J.C., Lagace P.A., “Quadratic stress criteria for the initiation of delamination”, *Journal of Composite Materials*, Vol. 22, pp. 1141-1155, 1988

[11] *Abaqus® Theory and User’s Manuals*, Hibbit, Karlsson & Sorensen, Pawtucket, USA, 2004.

[12] Whitney J. M., Browning C. E., “On short-beam tests for composite materials”, *Experimental Mechanics*, Vol. 25, pp. 294-300, 1985.

[13] ASTM, “ Standard test method for short beam strength of polymer composte material and their laminates”, ASTM D2344/ASTM D2344M-00 (Reapproved 2006).